Available online at www.sciencedirect.com
ScienceDirect
Trans. Nonferrous Met. Soc. China 24(2014) 1032−1038
Transactions of Nonferrous Metals Society of China
www.tnmsc.cn

# Laser-weldable $Si_p$−$SiC_p$/Al hybrid composites with bilayer structure for electronic packaging

Meng-jian ZHU, Shun LI, Xun ZHAO, De-gan XIONG

College of Aerospace Science and Engineering, National University of Defense Technology, Changsha 410073, China

Received 13 May 2013; accepted 8 July 2013

**Abstract:** Laser-weldable $Si_p$−$SiC_p$/Al hybrid composites with high volume fraction (60%−65%) of SiC reinforcement were fabricated by compression moulding and vacuum gas pressure infiltration technology. Microscopic observation displayed that the $Si_p$−$SiC_p$/Al hybrid composites with bilayer structure were compact without gas pores and the intergradation between $Si_p$/Al layer and $SiC_p$/Al layer was homogeneous and continuous. Further investigation revealed that the $Si_p$−$SiC_p$/Al hybrid composites possessed low density (2.96 g/cm$^3$), high gas tightness (1.0 mPa·cm$^3$)/s), excellent thermal management function as a result of high thermal conductivity (194 W/(m·K) and low coefficient of thermal expansion ($7.0\times10^{-6}$ K$^{-1}$). Additionally, $Si_p$−$SiC_p$/Al hybrid composites had outstanding laser welding adaptability, which is significantly important for electronic packaging applications. The gas tightness of components after laser welding (48 mPa·cm$^3$)/s) can well match the requirement of advanced electronic packaging. Several kinds of these precision components passed tests and were put into production.

**Key words:** $Si_p$−$SiC_p$/Al hybrid composites; laser welding; thermo-physical properties; electronic packaging

## 1 Introduction

For the excellent properties including high thermal conductivity (TC), low tunable coefficient of thermal expansion (CTE), high modulus and low density, high volume fraction (60%−75%) of SiC reinforcement, Al-matrix composites ($SiC_p$/Al) have become a new generation of electronic packaging materials [1−4]. $SiC_p$/Al composites are widely used as thermal management in the packaging of microwave, microelectronic and photoelectronic components, which will gradually replace the first generation (Kovar) and second generation (W−Cu, Mo−Cu) electronic packaging alloys in the near future [5].

However, the industrialization of $SiC_p$/Al composites is restricted by welding technique [6]. Aluminium is usually covered with a thin oxide film which blocks surface wetting of Al/SiC interface. Brazing, the most common welding method in past researches, always results in a reduction of gas tightness and reliability due to adding another kind of material besides the composites and cover plates [7]. Additionally, brazing is inefficient in industrialized production for its complicated procedures and parameters. Laser welding, which possesses several attractive advantages such as high efficiency, narrow heat-affected zone (HAZ) and minimal deformation, has a great potential in the field of electronic packaging. However, laser welding for $SiC_p$/Al composites usually forms gas pores and other defects around the weld zone because of the great difference in physical properties between Al-matrix and SiC reinforcement [8−11]. Furthermore, serious interface reaction always brings brittle phase $Al_4C_3$, which is the main cause of bad compactness and poor mechanical properties of weld joint [11,12].

More recently, we have developed a novel compression moulding technology [13], which was used in fabrication of Si−SiC preforms with accurate bilayer structure. After that, Al alloy was infiltrated into the Si−SiC preforms by vacuum gas pressure infiltration [14,15]. By adopting a series of developed techniques, the laser-weldable $Si_p$−$SiC_p$/Al hybrid composites with bilayer structure were made into near-net-shape precision components. This work will apart from brief description of the fabrication technology and present microstructures and properties of laser-weldable $Si_p$−$SiC_p$/Al hybrid composites.

**Corresponding author:** Xun ZHAO; Tel: +86-731-84574187; E-mail: xzhao56@126.com
DOI: 10.1016/S1003-6326(14)63158-7

## 2 Experimental

The flowchart of the experimental procedures in this study is given in Fig. 1.

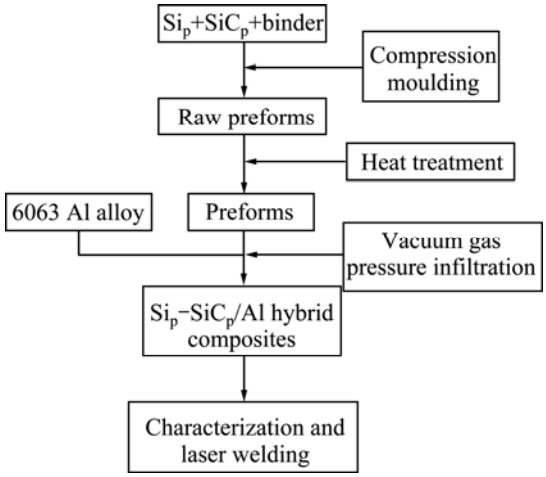


**Fig. 1** Flowchart of preparation and characterization of $Si_p$−$SiC_p$/Al hybrid composite components

### 2.1 Fabrication of bilayer Si−SiC preforms

In order to get preforms with high volume (60%−65%) of SiC reinforcement, SiC particles with different sizes (Fig. 2(a)) were well-distributed in the 3D mixer by mixing for 2 h, and then mixed with the binder system (polycarbosilane and paraffin, dissolved in gasoline). Finally, the uniformly mixed SiC particles were obtained after drying and screening out. The mixed Si particles (Fig. 2(b)) were treated by the similar procedures.

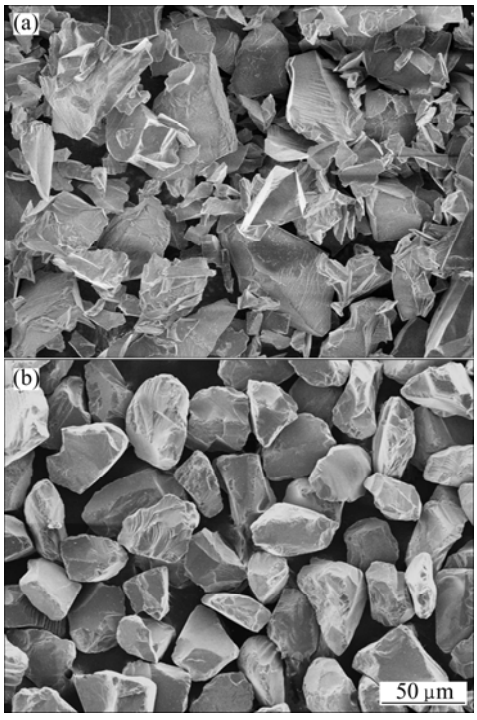


**Fig. 2** SEM images of reinforcement particles: (a) SiC particles; (b) Si particles

SiC particles and Si particles were processed to raw preform under the particular pressure of 200 MPa, and then heated to 800 °C and maintained for 2 h and cooled to room temperature under protection of $N_2$ in order to obtain the bilayer Si−SiC preforms (see Fig. 3).

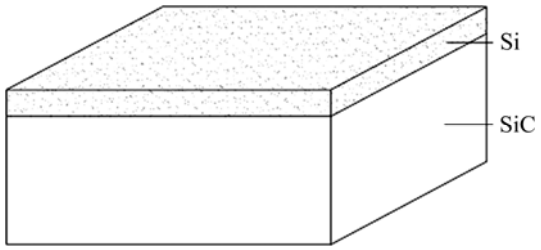


**Fig. 3** Schematic structure of bilayer Si−SiC preform

### 2.2 Preparation of $Si_p$−$SiC_p$/Al hybrid composites

6063 Al alloy was used as matrix metal fixed in the lower furnace while preforms were fixed in the upper furnace. Infiltration was carried out in a vacuum gas pressure apparatus. The temperatures of the lower and upper furnaces were 700 and 650 °C, respectively. Vacuum was applied until a pressure of 40 Pa was reached before heating. The infiltration pressure was increased to 12 MPa and maintained for 30 min under the protection of $N_2$. Melt Al alloy was infiltrated into preforms and solidification occurred right way. After cooling to room temperature, the $Si_p$−$SiC_p$/Al hybrid composites were removed from the furnace and sampled for characterization of microstructure and properties.

The microstructure and fracture morphology of composites were observed by Axio Scope microscope (Carl Zeiss Corp.) and S−4800 scanning electronic microscope (Hitachi Corp.). The bending strength was tested using three-point bending on the WDW−100 electronic multi-purpose testing machine. The thermal conductivity (TC) and CTE were determined using LFA 447 (Netzsch Corp.) by flash laser method [16] and DIL 402 PC (Netzsch Corp.) respectively. The gas tightness was measured using helium mass spectrometry leak detector ZQJ−542 (KYKY Corp.). The bending and CTE specimens were in rectangles with dimensions of 40 mm × 4 mm × 4 mm and 25 mm × 4 mm × 4 mm, respectively. The specimen for thermal diffusivity measuring was a disk with diameter of 12 mm and thickness of 3 mm. The density was measured by the Archimedes' method.

### 2.3 Laser welding

The $Si_p$−$SiC_p$/Al hybrid composites have managed to be made into near-net-shape components (see Fig. 4). In order to obtain the components with accurate size and

shape, precision machining was accomplished on a series of numerical controlled machine tools. After being cleaned in acetone, the $Si_p$−$SiC_p$/Al hybrid composite components were packaged with the cover boards (4047 Al alloy) by laser welding. YAG solid pulsed laser welding machine was used under the protection of He atmosphere, in which the output power, laser frequency and welding speed were 2 kW, 40 HZ and 5 mm/s, respectively. Finally, the microstructure of welds and the gas tightness of packaged components after laser welding were determined by SEM, EDX and He mass spectrometry leak detector.

## 3 Results and discussion

Table 1 lists the typical properties of 63% $Si_p$−$SiC_p$/Al hybrid composites determined in this study, and Table 2 makes a comparison of the properties between 63% $Si_p$−$SiC_p$/Al hybrid composites and other materials for electronic packaging. Compared with other packaging materials, $Si_p$−$SiC_p$/Al hybrid composites, with lower density and more excellent thermal conductivity, can better match the requirement of advanced electronic components.

### 3.1 Microstructure and strength

Figure 5 shows metallographic micrograph of 63% $Si_p$−$SiC_p$/Al hybrid composites obtained in this work, which reveals a compact and homogeneous microstructure without pores. Figures 5 (a) and (b) illustrate the homogeneous distribution of both SiC particles and Si particles in the Al-matrix by optical microscope, while Fig. 5(b) shows a well distribution of SiC particles in aluminum matrix that demonstrated by the SEM micrographs. Almost, molten metal was infiltrated in the pores under the applied vacuum and gas pressure during the infiltrating process. For infiltration of molten aluminum into the pores, 6063 Al-matrix seems like a network structure among the reinforcement particles. Due to a one-off compression moulding of $Si_p$−$SiC_p$ preform, the intergradation of $Si_p$/Al−$SiC_p$/Al is homogeneous and continuous, as shown in Fig. 5(d).

Examination of the fracture surfaces produced during three-point flexural testing reveals that the cracks pass through the SiC particles and Al-matrix without observation of the debonding of Al−SiC interface. The fracture micrographs (see Fig. 6) clearly show that almost all the SiC particles on the fracture surfaces belong to the cracked particles rather than debonded ones and the most of particles run parallel to the fracture surfaces of the composites. This mode of fracture indicates that the failure is dominantly caused by the SiC particles fracture and Al-matrix dimple rapture rather than by the interface debonding, which means that the interface bonding between Al-matrix and SiC reinforcement is significantly strong.

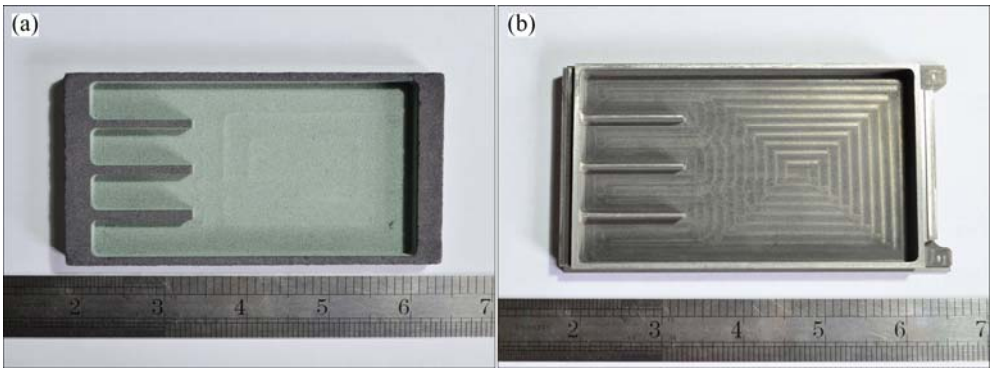


**Fig. 4** Si−SiC preform (a) and $Si_p$−$SiC_p$/Al hybrid composite component (b)

**Table 1** Properties of 63% $Si_p$−$SiC_p$/Al hybrid composites

| Density/ ($g·cm^{-3}$) | Thermal conductivity/ ($W·m^{-1}·K^{-1}$) | CTE/$10^{-6}K^{-1}$ | Gas tightness/ ($mPa·cm^3·s^{-1}$) | Elastic modulus/GPa | Bending strength/MPa |
|---|---|---|---|---|---|
| 2.96 | 204 | 7.0 | 1.0 | 235 | 336 |

**Table 2** Comparison of properties with other materials

| Material | $\rho$/($g·cm^{-3}$) | $\lambda$/($W·m^{-1}·K^{-1}$) | CTE/$10^{-6}K^{-1}$ | Elastic modulus/GPa |
|---|---|---|---|---|
| Kovar alloy [17] | 8.36 | 17 | 6.0 | 131 |
| 15%Cu/85%W [18] | 16.4 | ~180 | 6.5 | 334 |
| 20%Cu/80%Mo [19] | 9.95 | ~150 | 7.4 | 200 |
| 63% $Si_p$−$SiC_p$/Al | 2.96 | 204 | 7.0 | 235 |

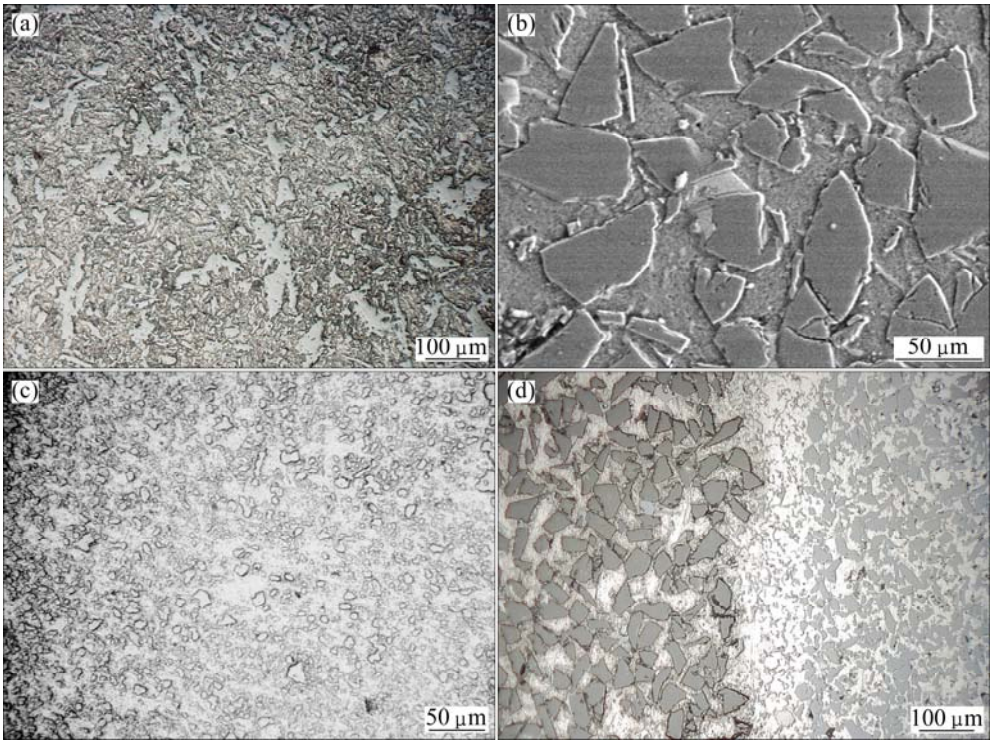


**Fig. 5** Optical images of 63% $Si_p$−$SiC_p$/Al hybrid composites: (a) SiC/Al layer; (b) SiC distribution; (c) $Si_p$/Al layer; (d) Interface between $SiC_p$/Al layer and Si/Al layer

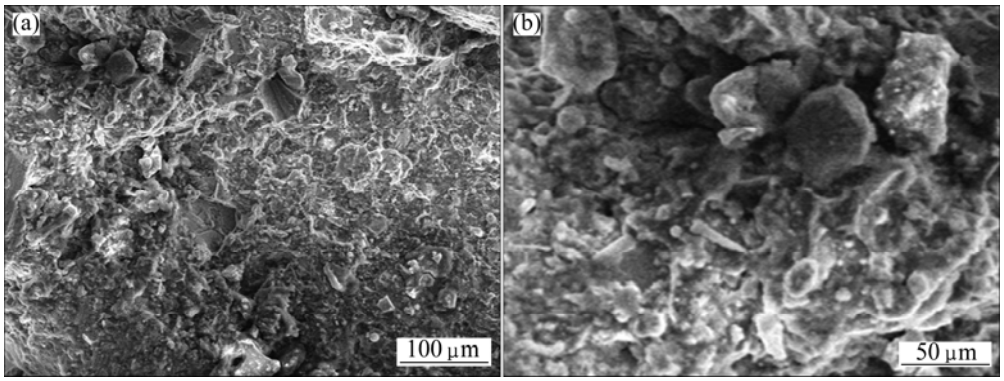


**Fig. 6** SEM images showing fracture surface of $Si_p$−$SiC_p$/Al hybrid composites with different magnifications

### 3.2 Thermal conductivity and coefficient of thermal expansion

Figure 7 shows the thermal conductivity (TC) of $Si_p$−$SiC_p$/Al hybrid composites at different temperatures ranging from 25 to 200 °C. The comparison among $Si_p$−$SiC_p$/Al hybrid composites and Al-matrix and $SiC_p$/Al composites produced by CPS Corporation (USA) [20] was also illustrated in this study.

Compared with the initial thermal conductivity of 230 W/(m·K) at 25 °C, when heating up to 200 °C, the thermal conductivity of Al-matrix slowly decreased to 218 W/(m·K). The drop of thermal conductivity of Al-matrix was less than 7%. In contrast, the thermal conductivity of $Si_p$−$SiC_p$/Al hybrid composites declined from 194 to 150 W/(m·K), during which the reduction was about 25%. This difference could be

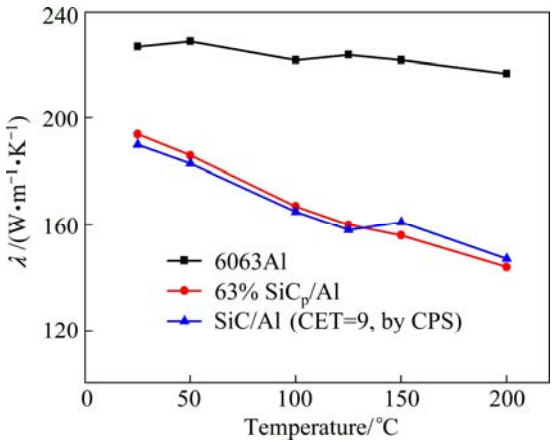


**Fig. 7** Thermal conductivity of Al-matrix, $SiC_p$/Al composites and $Si_p$−$SiC_p$/Al hybrid composites

explained in terms of coefficient of thermal expansion (CTE) and elastic modulus. With the increase of temperature, the CTE of Al-matrix increased and the elastic modulus declined, while the CTE and elastic modulus of SiC particles remained steady under 200 °C. The stress of Al−SiC interface became larger and the combination was weaker, which makes heat transfer in composites more difficult. Because the thermal conductivity of A6063 Al-matrix was higher compared with A356 Al-matrix, the thermal conductivity of $Si_p$−$SiC_p$/Al hybrid composites was a little higher than that of $SiC_p$/Al composites produced by CPS corporation at different temperatures. Additionally, the further research from CPS corporation also revealed that the reduction of thermal conductivity was slight when the temperature was higher than 200 °C and still remained at 134 W/(m·K) when temperature reached 300 °C.

Figure 8 shows the CTE of Al-matrix and $Si_p$−$SiC_p$/Al hybrid composites respectively at temperatures ranging from 100 to 500 °C. CTE of Al-matrix increased with the increasing temperature before 350 °C. The average distance between $\alpha$(Al) atoms in crystal lattice was enlarged by the intensified lattice vibration, which impaired the metallic bonds and elastic modulus and finally resulted in the growth of CTE. However, CTE of Al-matrix slightly fell down when temperature was higher than 400 °C. This deregulation could be explained by the increasing solubility of silicon and magnesium in $\alpha$(Al) crystal at high temperatures, which reduced the lattice constant of $\alpha$(Al) crystal.

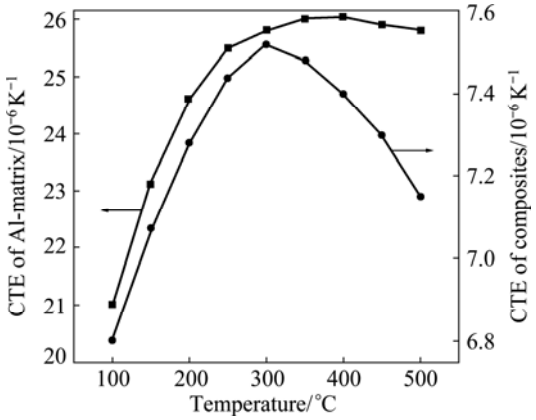


**Fig. 8** CTE of A6063 Al-matrix and 63%$Si_p$−$SiC_p$/Al hybrid composites

For the composites, the $Si_p$−$SiC_p$/Al hybrid growth of CTE before approximately 300 °C also could be demonstrated by above similar theories. Due to a lower CTE ($4.35\times10^{-6}$ $K^{-1}$), high volume fraction of SiC reinforcement with pseudo network structure restricts the thermal expansion of composite itself, which well explains the slower growth of CTE of composites compared with Al-matrix. When temperature exceeded 300 °C, with the decrease of elastic modulus and bending strength of Al-matrix, the restriction was more apparent than before, which reduced the CTE of composites at higher temperatures. The maximum CTE of $Si_p$−$SiC_p$/Al hybrid composite was $7.5\times10^{-6}$ $K^{-1}$ at 300 °C.

It is clearly shown in Fig. 8, CTE of $Si_p$−$SiC_p$/Al hybrid composites is between $6.8\times10^{-6}$ $K^{-1}$ and $7.5\times10^{-6}$ $K^{-1}$ in the temperature range of 100−500 °C, which well matches the expansion of LTCC (low temperature co-fired ceramic) [21] substrates and GaAs chips and consequently reduces the thermal stress in electronic packaging.

### 3.3 Laser welding

YAG solid pulsed laser welding machine was used in this study and the output power, laser frequency and welding speed during laser welding were 2 kW, 40 HZ and 5 mm/s, respectively. In order to achieve the satisfied properties of composite component, especially the gas tightness, laser welding was accomplished after the components were black treated by graphite and carbon black under the protection of He atmosphere. Figure 9 illustrates the microstructure of weld, in which a compact and homogeneous structure of weld formed without apparent pores and deformation. Before laser welding, the base matrix consists of $Si_p$/Al composites and 4047 Al alloy. EDS analysis was used to describe the composition of weld. The result shows that O, Fe and Mg elements exist in the weld zone in addition to Al and Si (see Table 3). Compared with the laser welding of $SiC_p$/Al composites, there is no brittle phase $Al_4C_3$ formed which is quite harmful to the strength and gas tightness of weld joint.

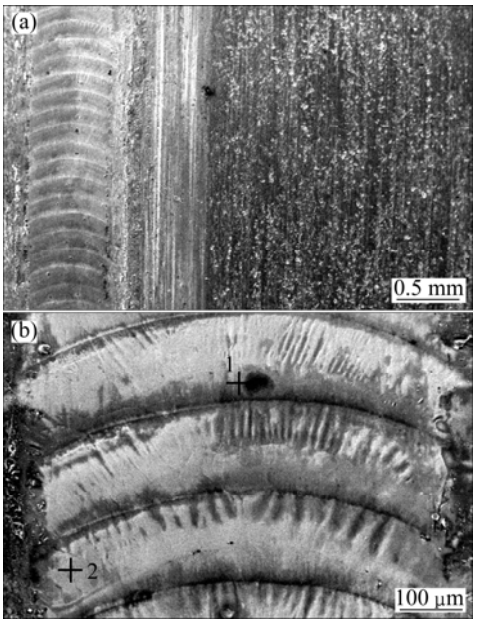


**Fig. 9** Optical images of weld joint of Si−SiC/Al hybrid composites with different magnifications

**Table 3** EDS analysis results of areas 1 and 2 in Fig. 9(b)

| Area | $w$(Al)/% | $w$(Si)/% | $w$(O)/% | $w$(Fe)/% | $w$(Mg)/% |
|---|---|---|---|---|---|
| 1 | 75.097 | 22.521 | 2.048 | 0.357 | 0.057 |
| 2 | 82.490 | 14.869 | 1.664 | 0.872 | 0.103 |

Due to lower output power (2 kW) and higher welding frequency (40 Hz), the distortion of $Si_p$−$SiC_p$/Al hybrid composites component after laser welding, which was caused by the CTE difference between $Si_p$/Al (CTE: $15\times10^{-6}$ $K^{-1}$) and $SiC_p$/Al (CTE: $7\times10^{-6}$ $K^{-1}$), was controlled to be a reasonable level.

Figures 10 and 11 show the effects of surface treatment and protective gas on gas tightness of welded joint, respectively.

The initial gas tightness of $Si_p$−$SiC_p$/Al hybrid composites is 1.0 mPa·cm$^3$/s. The gas tightness of polished surface is 120 mPa·cm$^3$/s, and reduced to 76 mPa·cm$^3$/s after specimens were cleaned with acetone with acetone. This reduction could be explained by different absorption of surface to laser, which is lower for polished shining surface. After being cleaned with acetone, specimens were black treated by sand blasting and graphite. The gas tightness is 48 mPa·cm$^3$/s.

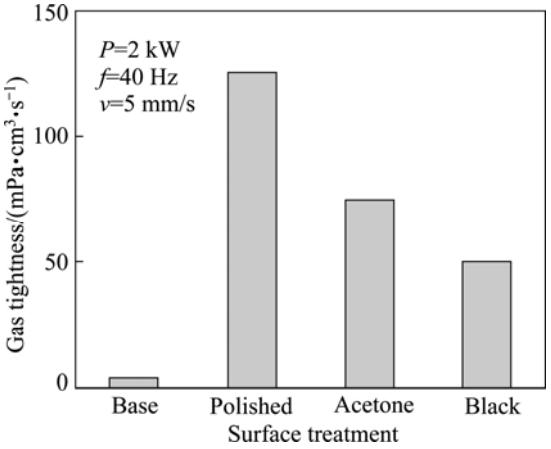


**Fig. 10** Effects of surface treatment on gas tightness of weld joint

During the laser welding, four kinds of different protective gases, argon, compressed air, $CO_2$ and helium were used to protect weld zone from the attacking of oxidation reactions oxidation and forming plasma. A high ionization potential of He makes it hard to form plasma during laser welding and then obviously improves the gas tightness (48 mPa·cm$^3$/s) of weld joint. On the contrary, Ar has lower ionization potential which caused a bad condition of gas tightness (97 mPa·cm$^3$/s). The effects of compressed air and $CO_2$ on gas tightness of weld joint are better than the effect in argon and worse than in helium gas while keeping other conditions unchanged. Further studies [22] also reveal that adding appropriate Ar (volume fraction of 10%) into He will get an optimal quality of laser welding, which could be explained by the fact that it is hard to totally expel the air around the weld zone by helium gas (lighter atom compared with air) in a short time and thus adding argon gas will be more use full.

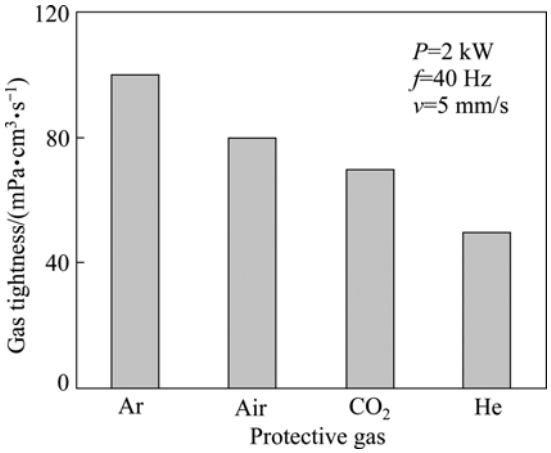


**Fig. 11** Effects of protective gas on gas tightness of weld joint

## 4 Conclusions

1) High reinforcement content $Si_p$−$SiC_p$/Al hybrid composites (volume fraction of 60%−65%) were fabricated by compression moulding and vacuum gas pressure infiltration technology.

2) 63% $Si_p$−$SiC_p$/Al hybrid composites possess excellent properties, low density (2.96 g/cm$^3$), high thermal conductivity (204 W/(m·K)), low CTE ($7.0\times10^{-6}$ $K^{-1}$) and good gas tightness after laser welding (48 mPa·cm$^3$/s).

3) Laser welding between $Si_p$−$SiC_p$/Al hybrid composites and 4047 Al alloy cover plates was successfully accomplished using YAG solid pulse laser welding machine. The most suitable parameters of laser welding are 2 kW of output power, 50 Hz of laser frequency and 5 mm/s of welding speed.

4) The weld of composite component is compact and homogeneous without gas pores and no brittle phase ($Al_4C_3$) is observed. During the laser welding process, black treatment by graphite and protection under He atmosphere is quite beneficial to improve the gas tightness of packaged components.

## References

[1] ZWEBEN C. Advanced electronic packaging materials: Advanced Materials and Processes [J]. JOM, 2005, 163: 33−37.

[2] TERRY B, JONES G. Metal matrix composites: Current developments and future trends in industrial research and applications [M]. Amsterdam: Elsevier Publishers, 1990.

[3] PECH-CANUL M I, MAKHLOUF M M. Processing of Al−$SiC_p$ metal matrix composites by pressureless infiltration of SiC performs [J]. Journal of Materials Synthesis and Processing, 2000, 8: 35−53.

[4] LEE H S, JEON K Y, KIM H Y. Fabrication process and thermal properties of SiCp/Al metal matrix composites for electronic packaging applications [J]. Journal of Materials Science, 2000, 35: 6231−6236.
[5] TUMMALA R R. Ceramic and glass-ceramic packaging in the 1990s [J]. Journal of the American Ceramic Society, 1991, 73: 895−908.
[6] ELLIS M B D. Joining of Al base metal matrix composites [J]. International Materials Reviews, 1996, 42: 41−58.
[7] ZHANG X P, QUAN G F, WEI W. Preliminary investigation on joining performance of $SiC_p$-reinforced Al metal matrix composite (Al−$SiC_p$-MMC) by vacuum brazing [J]. Composites A, 1999, 30: 823−827.
[8] DAHOTRE N B, NAREBDRA B, MCCAY M H. Pulse laser processing of a SiC/Al-alloy metal matrix composites [J]. Journal of Materials Research, 1991, 6: 514−529.
[9] DAHOTRE N B, MCCAY M H. Laser welding of a SiC/Al-alloy metal matrix composites [J]. Laser Institute of America, 1991, 71: 343−356.
[10] YUE T M, XU J H, MAN H C. Pulse Nd-YAG laser welding of a SiC particles reinforced aluminium alloy composites [J]. Applied Composite Materials, 1997, 4: 53−64.
[11] NIU Ji-tai. Research on laser welding of aluminium matrix composites: $SiC_w$/6061Al MMC [J]. Vacuum, 2006, 80: 1396−1399.
[12] URENA A, ESCALERA M D, GIL L. Influence of interface reaction on fracture mechanisms in TIG arc-welded Al matrix composites [J]. Composites Science and Technology, 2000, 60: 613−622.
[13] XIONG De-gan. Study on the preparation and properties of AlSiC electronic packaging materials and typical component [D]. Changsha: National University of Defense Technology, 2009. (in Chinese)
[14] SONG Min. Effects of volume fraction of SiC particles on mechanical properties of SiC/Al composites [J]. Transactions of Nonferrous Metals Society of China, 2009, 19: 1400−1404.
[15] ALPTEKIN K. Infiltration of A6063 aluminium alloy into SiC−$B_4C$ hybrid preforms using vacuum assisted block mould investment casting technique [J]. Transactions of Nonferrous Metals Society of China, 2012, 22: 1563−1567.
[16] PAKE W J, JENKINS R J, BULTER C P. Flash method of determining thermal diffusivity, heat capacity and thermal conductivity [J]. Journal of Applied Physic, 1961, 32: 1679−1684.
[17] ZANCHETTA A, LEFORT P, GRABBAY E. Thermal expansion and adhesion of ceramic to metal sealing: case of porcelain-Kovar junctions [J]. Journal of European Ceramic Society, 1995, 15: 233−238.
[18] LIU Bin-bin, XIE Jian-xin, CHEN Jiang-hua. Thermo-physical properties of W−Cu functionally gradient materials [J]. The Chinese Journal of Nonferrous Metals, 2009, 19(3): 538−543. (in Chinese)
[19] CHEN Guo-qin, ZHU De-zhi, ZHAN Rong, ZHANG Qiang, WU Gao-hui. Highly dense Mo/Cu composites fabricated by squeeze casting and their thermal conduction properties [J]. The Chinese Journal of Nonferrous Metals, 2005, 15(11): 1864−1868. (in Chinese)
[20] ZHU Xiao-min, YU Jia-kang, WANG Xin-yu. Microstructure and properties of Al/Si/SiC composites for electronic packaging [J]. Transactions of Nonferrous Metals Society of China, 2012, 22(7): 1686−1692.
[21] LI Ting-ting, PENG Chao-qun, WANG Ri-chu, WANG Xiao-feng, LIU Bing. Research progress in ceramic substrate materials for electronic packaging [J]. The Chinese Journal of Nonferrous Metals, 2010, 20: 1365−1373. (in Chinese)
[22] WANG X H, NIU J T, GUAN S K. Investigation on TIG welding of $SiC_p$-reinforced Al-matrix composites using shielding gas and Al−Si filler [J]. Materials Science and Engineering A, 2009, 499: 106−110.

# 具有双层结构的电子封装用可激光焊接 $Si_p$−$SiC_p$/Al 混杂复合材料

朱梦剑，李 顺，赵 恂，熊德赣

国防科学技术大学 航天科学与工程学院，长沙 410073

**摘 要**：结合预制件一次性模压成型和真空气压浸渗技术制备具有双层结构的高体积分数(60%~65%)、可激光焊接 $Si_p$−$SiC_p$/Al 混杂复合材料。该复合材料的组织结构均匀、致密，增强相颗粒均匀地分布在复合材料中，$Si_p$/Al−$SiC_p$/Al 界面均匀、连续、结合紧密。性能测试表明，$Si_p$−$SiC_p$/Al 混杂复合材料具有密度低(2.96 g/$cm^3$)、热导率高(194 W/(m·K))、热膨胀系数小($7.0\times10^{-6}K^{-1}$)、气密性好 ($1.0\times10^{-3}$ (Pa·$cm^3$)/s)等优异特性。焊接试验表明，$Si_p$−$SiC_p$/Al 混杂复合材料具有良好的激光焊接特性，其焊缝平整、致密，微观组织均匀，没有生成明显的气孔和脆性相 $Al_4C_3$。同时，$Si_p$−$SiC_p$/Al 混杂复合材料激光封焊后优异的气密性($4.8\times10^{-2}$ (Pa·$cm^3$)/s)能够满足现代电子封装行业对气密性的严格要求。

**关键词**：$Si_p$−$SiC_p$/Al 混杂复合材料；激光焊接；热物理性能；电子封装

**(Edited by Xiang-qun LI)**